

A model-free direct predictive grid-current control strategy for grid-connected converter with an inductance-capacitance-inductance filter

LEILEI GUO¹, MINGZHE ZHENG¹  , CHANGZHOU YU², HAIZHEN XU², YANYAN LI¹

¹Zhengzhou University of Light Industry, College of Electrical and Information Engineering
China

²Hefei University, School of Advanced Manufacturing Engineering
China

e-mail: 2006guoleilei[✉]zhengmingzhe32016}@163.com

(Received: 06.04.2022, revised: 26.09.2022)

Abstract: The disadvantages of the conventional model predictive current control method for the grid-connected converter (GCC) with an inductance-capacitance-inductance (LCL) filter are a large amount of calculation and poor parameter robustness. Once parameters of the model are mismatched, the control accuracy of model predictive control (MPC) will be reduced, which will seriously affect the power quality of the GCC. The article intuitively analyzes the sensitivity of parameter mismatch on the current predictive control of the conventional LCL-filtered GCC. In order to solve these issues, a model-free predictive current control (MFPCC) method for the LCL-filtered GCC is proposed in this paper. The contribution of this work is that a novel current predictive robust controller for the LCL-filtered GCC is designed based on the principle of the ultra-local model of a single input single output system. The proposed control method does not require using any model parameters in the controller, which can effectively suppress the disturbances of the uncertain parameter variations. Compared with conventional MPC, the proposed MFPCC has smaller current total harmonic distortion (THD). When the filter parameters are mismatched, the control error of the proposed method is smaller. Finally, a comparative experimental study is carried out on the platform of Typhoon and PE-Expert4 to verify the superiority and effectiveness of the proposed MFPCC method for the LCL-filtered GCC.

Key words: grid-connected converter (GCC), model-free predictive current control (MFPCC), parameter mismatch, robustness



1. Introduction

In recent years, with the rapid development of renewable energy distributed power generation systems, the grid-connected converter (GCC) has become a research hotspot in the field of power electronics [1, 2]. The GCC can efficiently convert direct current (DC) energy into alternating current (AC) energy, which is very important for renewable energy and microgrid systems. However, it is necessary to limit the harmonic of grid-connected current. Therefore, the converter needs to be connected to the power grid through a filter. Compared to the conventional inductance (L) filter, the inductance-capacitance-inductance (LCL) filter is widely used because it has higher high-frequency attenuation characteristics and can better suppress grid-current harmonics [3]. However, the LCL filter needs to have an option of an additional resonance suppression strategy because of the resonance spike problem [4–8].

At the same time, the improved computational speed of modern digital signal processors (DSPs) enables some modern control strategies, such as deadbeat control [9], adaptive control [10], sliding mode control [11], model predictive control (MPC) [5, 12] and so on, which have been applied to control GCCs. Among them, MPC is widely used in power converters due to the following advantages: simple and intuitive system design, a fast dynamic response system and multiple nonlinear target control [13, 14]. MPC has emerged as a useful algorithm for implementing LCL-filtered GCC control with considerable potential. A multi-step MPC method for a three-phase GCC with LCL-filter is proposed in [15]. The state variable error and switching state variation at multiple sampling times are added to the cost function at the same time, which plays a crucial role in tracking the state variable and reducing the switching frequency. Similarly, the multivariable approaches to MPC $i_1i_2u_c$ and MPC $i_1i_2u_c - 2$ steps are proposed in [4]. To ensure the excellent control effect of MPC, it is also essential to increase the stability of the system. The different state feedback methods for three-phase GCCs with LCL filters are studied deeply in [5]. This paper not only achieves multivariable control and low switching loss, but also introduces different active damping (AD) methods. However, none of these studies considered the influences of the model parameter mismatches.

As is well-known, the future prediction behavior of the GCC control system is based on the system specific model. So, the control performance of MPC is vulnerable to parameter changes and model uncertainty [16]. Especially in the steady state, reactor saturation, temperature change or aging of electrical elements will affect the prediction accuracy of the prediction model. The model parameter error will distort the grid-current under the MPC strategy [16–18]. Therefore, many scholars have also carried out relevant research to improve the parameter robustness of MPC in recent years.

A model error compensation scheme suitable for the MPC of three-phase converters is proposed in [19], it improves the control performance of the system rapidly. In order to further improve the dynamic and steady-state performance of the control system, an integrator is added to the output system to modify the dynamic performance and ensure zero steady-state errors under parameter errors in [20]. Though this approach overcomes the disadvantage that the conventional MPC strategy relies on a model with precise parameters, its application range is limited due to the introduction of a linear controller. In [21], an adaptive reference MPC scheme is proposed, which can significantly attenuate the steady-state deviation in the system and the performance is better than MPC with an integrator under the condition of model mismatches. Similarly, an adaptive

discrete time MPC system is also proposed based on the model reference adaptive method, which further improves the control performance of the system in [22].

To thoroughly enhance the parameter robustness of MPC when the load model is uncertain, model-free predictive control has attracted extensive attention in recent years. Model-free predictive current control (MFPCC) was proposed for the first time in [23], it is simple and easy to implement. Considering the system parameter uncertainty and converter nonlinearity, the idea of a data-driven ultra-local model has been widely used in converter control in recent years [24–26]. In [26], model-free predictive control is applied to doubly-fed wind turbines, which can also achieve a good control effect. However, the above literature only studies the model-free predictive control of single input-output first-order systems [23–26]. At present, the model-free direct predictive grid-current control of GCCs based on LCL filters has not been studied, which is a high order system.

To improve the dynamic performance and steady-state control accuracy of the LCL-filtered GCC, and enhance the robustness against the change of model parameters, this paper innovatively combines model-free control with current predictive control to establish a third-order MFPCC controller. Moreover, an active damping scheme is studied to suppress the inherent resonance peak of the system. The proposed method can not only realize model-free predictive control of grid current and enhance parameter robustness, but also reduce grid-current harmonics and improve grid connected power quality. The experimental results verify the effectiveness of the proposed method.

2. Conventional model predictive grid-current control

This section introduces the system model of the LCL-filtered GCC and the conventional MPC method. The influence of filter parameter mismatches on the grid-current control is discussed in the next section.

2.1. Topology of the GCC with LCL filter

Figure 1 shows the typical topology of a GCC with a LCL filter. Here, U_{dc} is the input DC

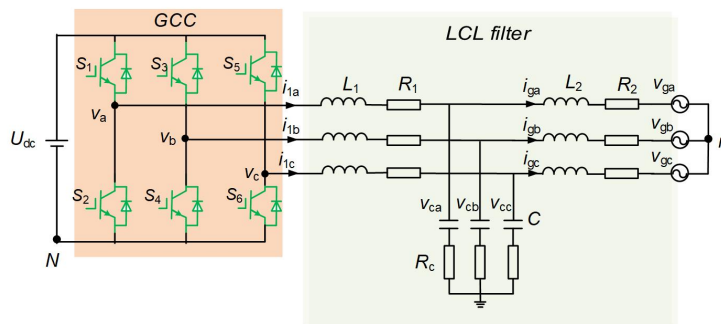


Fig. 1. Typical topology of a GCC with LCL filter

voltage, $S_1 \sim S_6$ are the six IGBT switches of the three-phase converter, R_1 is the internal resistance of the filter inductor L_1 on the converter side, R_2 is the internal resistance of the filter inductor L_2 on the grid side, and R_c is the passive damping resistance. L_1 , L_2 and C constitute the LCL filter. v_{an} , v_{bn} and v_{cn} represent the converter side voltage. v_{ca} , v_{cb} and v_{cc} represent the capacitor voltage of the filter. v_{ga} , v_{gb} and v_{gc} stand for the grid voltage. i_{1a} , i_{1b} , and i_{1c} represent the converter side current, and i_{ga} , i_{gb} and i_{gc} stand for the grid current.

2.2. Discrete prediction model of LCL-filtered GCC

Assuming that the three-phase grid voltage is balanced, according to Kirchhoff's law of voltage and current, the circuit equation of the three-phase LCL-filtered GCC is established, as well as the continuous-time state-space model form of a three-phase circuit as shown in (1), using the state matrix Φ_f , input matrix T_c and interference matrix T_{gc} . The state variables of the system are selected as $\mathbf{x} = [i_1, v_c, i_g]^T$.

$$\frac{d\mathbf{x}(t)}{dt} = \Phi_f \mathbf{x}(t) + T_c v_{inv}(t) + T_{gc} v_g(t) \quad (1)$$

with

$$\Phi_f = \begin{pmatrix} \frac{R_c + R_1}{-L_1} & \frac{1}{-L_1} & \frac{R_c}{L_1} \\ \frac{1}{C} & 0 & \frac{1}{-C} \\ \frac{R_c}{L_2} & \frac{1}{L_2} & \frac{R_c + R_2}{-L_2} \end{pmatrix}, \quad T_c = \begin{bmatrix} \frac{1}{L_1} \\ 0 \\ 0 \end{bmatrix}, \quad T_{gc} = \begin{bmatrix} 0 \\ 0 \\ \frac{1}{L_2} \end{bmatrix}, \quad (2)$$

where i_1 , i_g , v_{inv} , v_c and v_g are the vectors for three-phase converter-side current, grid-side output current, converter output voltage, filter capacitor voltage and grid voltage, respectively.

The continuous state equation of the system can be discretized accurately. Then, the discrete equation of the system is obtained as follows:

$$\mathbf{x}(k+1) = \Phi_{fd} \mathbf{x}(k) + T_{cd} v_{inv}(k) + T_{gcd} v_g(k) \quad (3)$$

with

$$\Phi_{fd} = e^{\Phi_f T}, \quad T_{cd} = \int_0^T e^{\Phi_f \delta} T_c d\sigma, \quad T_{gcd} = \int_0^T e^{\Phi_f \delta} T_{gc} d\sigma, \quad (4)$$

where Φ_{fd} , T_{cd} , and T_{gcd} are the constant predictive matrices. T is the sampling period. Equation (3) means that the state $\mathbf{x}(k+1) = [i_1(k+1), v_c(k+1), i_g(k+1)]^T$ of the system at the $(k+1)$ -th instant can be determined by the state $\mathbf{x}(k)$, the interference $v_g(k)$ and the system input $v_{inv}(k)$.

The control objective of an MPC algorithm is expressed by the cost function, which evaluates the control errors of each voltage vector. Finally, the voltage vector corresponding to the minimum g value is selected as the optimal voltage vector in the optimization process, and it is used to control the GCC. The cost function of conventional model predictive current control for a three-phase GCC with an LCL filter in the $\alpha\beta$ coordinate system can be defined as follows.

$$g = |i_{g\alpha}^*(k+1) - i_{g\alpha}(k+1)| + |i_{g\beta}^*(k+1) - i_{g\beta}(k+1)|, \quad (5)$$

where $i_{g\alpha}(k+1)$, $i_{g\beta}(k+1)$ are the grid-current state predictions by the predictive model (3). $i_{g\alpha}^*(k+1)$, $i_{g\beta}^*(k+1)$ are the reference grid current at $(k+1)$ -th in the stationary coordinate system, respectively.

However, Eq. (3) can't describe the system accurately. One of the main disadvantages is that there may be control errors when the filter parameters L_1 , L_2 and C in Φ_f , T_c , T_{gc} are inaccurate, and that will seriously affect the grid-connected power quality. To solve above problems, a model-free predictive grid-current control method is proposed in this paper.

3. Parameter sensitivity analysis

The above MPC method depends on the precision of the model. In other words, when the filter model parameters do not match the actual filter parameters, the control error will be increased. In terms of uncertainty of LCL filter parameters, the changes of the resistance R_1 , R_2 and R_c have little effect compared with filter inductance and filter capacitance. Therefore, only the error of filter inductance on the converter side L_{1e} , filter capacitance error C_e and filter inductance error L_{2e} on the grid side are considered, which can be expressed as

$$\begin{cases} L_{1e} = L_1^* - L_1 \\ C_e = C^* - C \\ L_{2e} = L_2^* - L_2 \end{cases}, \quad (6)$$

where: the converter side inductor L_1 , the filter capacitor C and the grid-side inductor L_2 are the actual filter parameters, respectively. L_1^* , C^* and L_2^* indicate the converter side inductance, filter capacitor and grid-side inductance used in the controller, respectively.

Equation (3) is formulated as (7) in the case of parameter mismatch.

$$\hat{x}(k+1) = \hat{\Phi}_{fd}x(k) + \hat{T}_{cd}v_{inv}(k) + \hat{T}_{gcd}v_g(k), \quad (7)$$

where

$$\begin{aligned} \hat{\Phi}_{fd} &= e^{\hat{\Phi}_f T}, \quad \hat{T}_{cd} = \int_0^T e^{\hat{\Phi}_f \delta} \hat{T}_c d\sigma, \quad \hat{T}_{gcd} = \int_0^T e^{\hat{\Phi}_f \delta} \hat{T}_{gc} d\sigma, \\ \hat{\Phi}_f &= \begin{pmatrix} \frac{R_c + R_1}{-(L_1 + L_{1e})} & \frac{1}{-(L_1 + L_{1e})} & \frac{R_c}{(L_1 + L_{1e})} \\ \frac{1}{C + C_e} & 0 & \frac{1}{-(C + C_e)} \\ \frac{R_c}{(L_2 + L_{2e})} & \frac{1}{(L_2 + L_{2e})} & \frac{R_c + R_2}{-(L_2 + L_{2e})} \end{pmatrix}, \\ \hat{T}_c &= \begin{bmatrix} 1 \\ (L_1 + L_{1e}) \\ 0 \\ 0 \end{bmatrix}, \quad \hat{T}_{gc} = \begin{bmatrix} 0 \\ 0 \\ 1 \\ -(L_2 + L_{2e}) \end{bmatrix}. \end{aligned}$$

When the filter parameters are mismatched, the control error of system state variables can be defined as

$$\boldsymbol{\varepsilon}_x = \widehat{\boldsymbol{x}}(k+1) - \boldsymbol{x}(k+1). \quad (8)$$

Since the control target is the grid current i_g , we will mainly analyze the prediction error of the grid current. The filter parameter L_1 , C , and L_2 have influence on the control performance of grid current. In order to analyze the current predictive control error more intuitively, three types of error mismatch are selected for analysis [16].

Firstly, when the converter side inductance and filter capacitor in the controller deviate from L_1 and C in the actual filter circuit, the grid-current predictive control error $\boldsymbol{\varepsilon}_{g1}$ is defined as $\boldsymbol{\varepsilon}_{g1} = \hat{i}_{g1}(k+1) - i_g(k+1)$.

Secondly, when the converter side inductance and grid-side inductance in the model deviate from L_1 and L_2 in the actual filter circuit, the prediction error of the grid-current $\boldsymbol{\varepsilon}_{g2}$ in the second case can be given by $\boldsymbol{\varepsilon}_{g2} = \hat{i}_{g2}(k+1) - i_g(k+1)$.

Last, when the filter capacitor and grid-side inductance in the model deviate from C and L_2 in the actual filter circuit, the grid-current predictive control error $\boldsymbol{\varepsilon}_{g3}$ is shown as $\boldsymbol{\varepsilon}_{g3} = \hat{i}_{g3}(k+1) - i_g(k+1)$.

It is worth highlighting that the prediction error is a complex vector that depends on instantaneous values of the converter side voltage $v_{inv}(k)$ and current $i_1(k)$, filter capacitor voltage $v_c(k)$, grid-side voltage $v_g(k)$ and current $i_g(k)$. In each sampling period, the load voltage source remains unchanged, but it needs to evaluate multiple voltage vectors of the converter output, which will produce different prediction errors. For single-vector MPC, there are eight different output voltages on each sampling period. The magnitude of voltage and current vectors and their relative directions in the complex plane, as well as the parameter errors of load resistance and inductance will lead to a variety of situations. Here, the output voltage vector $\boldsymbol{v}_{inv} = 2U_{dc}/3$ is selected as an example to analyze the prediction error. Figure 2 shows the prediction error for a range of load inductance and capacitance mismatch.

It can be seen from Fig. 2(a) that when $L_{1e} = 0$, $C_e = 0$, the absolute value of the prediction error $|\boldsymbol{\varepsilon}_{g1}| = 0$. It indicates that there is no prediction current control error when the converter side inductance and filter capacitor parameters match. However, with the increase or decrease of L_{1e} and C_e , the predictive current control error will increase. Especially, when L_{1e} and C_e decrease, the current predictive control error is larger. In Fig. 2(b), when the error between the converter side inductance L_{1e} and the grid-side inductance L_{2e} is zero, the predictive current control error $|\boldsymbol{\varepsilon}_{g2}| = 0$. Similarly, when the converter side inductance and the grid-side inductance are different from the actual value, the current prediction and control error will increase further. The influence of filter capacitance error C_e and grid-side inductance error L_{2e} on current predictive control error are depicted in Fig. 2(c). It can be observed that the variation of the grid-side inductance has a great influence on the current prediction error. The smaller the grid-side inductance is, the larger the prediction error is. Through the above analysis, it can be found that when the filter parameters are less than the actual circuit value (L_{1e} , C_e and L_{2e} are less than zero, respectively), the influence on the prediction current error is more obvious.

If other voltage vectors are selected as an example to analyze the prediction error, same conclusions can be drawn.

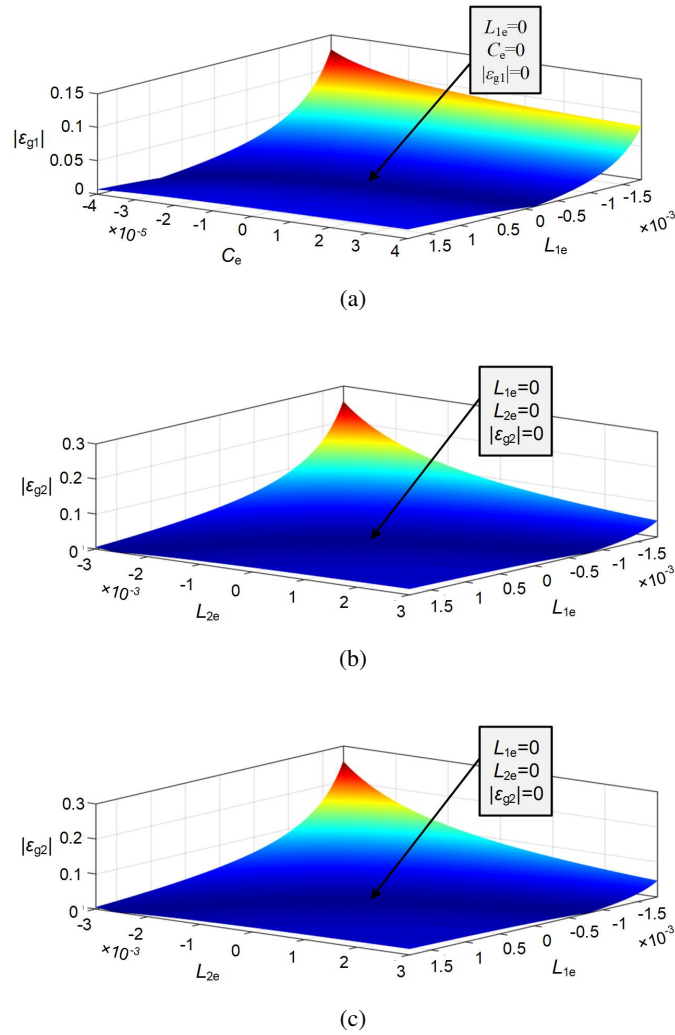


Fig. 2. Predictive control error of grid current: (a) the converter side inductance and filter capacitance deviate from the actual value; (b) the inductance of converter side and grid-side deviate from the actual value; (c) the filter capacitance and the grid-side inductance deviate from the actual value

4. MFPC of GCC with LCL filter

To enhance the robustness of the control parameters of the LCL-filtered GCC, and obtain considerable performance in the case of parameter misalignment, a model-free grid-current predictive control method is proposed and described as follows. The control diagram of the proposed MFPC is shown in Fig. 3.

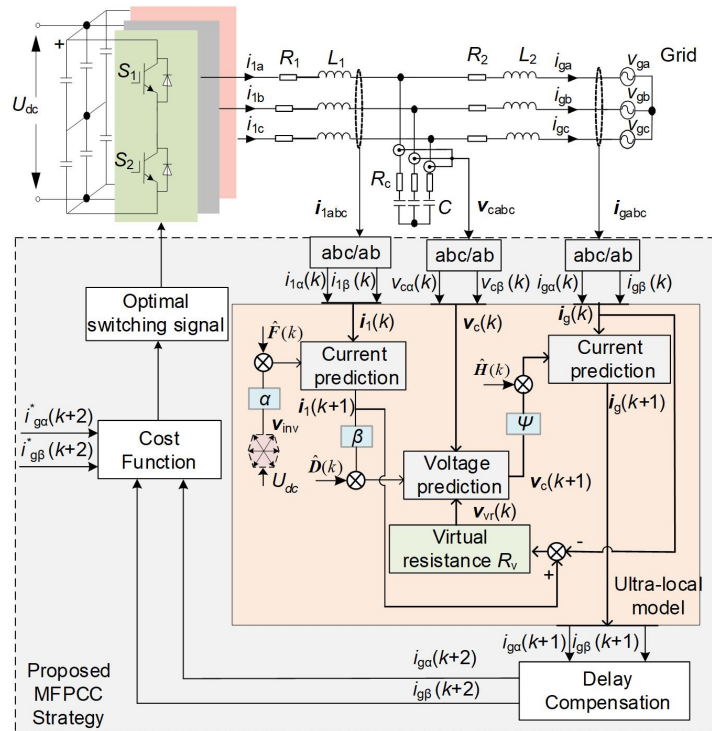


Fig. 3. MFPPC control structure of LCL-filtered GCC

Meanwhile, the designed virtual damping is also implemented concretely in MFPPC structure as shown in Fig. 3. On the basis of the original capacitor voltage predictive control, an inner capacitor current loop is added. The additional virtual resistance R_v will be realized in the form of an algorithm in the controller without increasing the circuit loss. At each sampling time, the capacitance current is obtained by the difference between the measured inverter current and grid current. When capacitor current crosses the virtual resistance R_v , the virtual capacitor voltage is output and applies to capacitor voltage predictive control. Finally, the predicted results are input to the MFPPC cost function, and the optimal switching sequence corresponding to the predicted value that minimizes the cost function is selected and directly acts on the LCL-filtered GCC as the control signals.

4.1. MFPPC of Grid current for LCL-filtered GCC

One of the main disadvantages of conventional MPC is its dependence on parameters (that is, the control accuracy of predictive current is closely related to the control parameters of load circuits). Once the parameters of the control model do not match the actual circuit parameters, the predictive control error will be generated and the power quality of grid current will be reduced. Therefore, it is necessary to study the predictive current robust control of the LCL-filtered GCC.

Based on the conventional MPC for the LCL-filtered GCC, the robust predictive control of grid-connected current is realized with the idea of an ultra-local model. In the case of parameter mismatch, the load dynamic equation of the three-phase LCL-filtered GCC based on the ultra-local model can be described as

$$\frac{dx}{dt} = \underbrace{\Phi_{fm} + T_{cm}v_{inv} + T_{gcm}v_g + \lambda m_v}_{\Gamma_m} \quad (9)$$

with

$$\Phi_{fm} = \begin{pmatrix} \frac{R_c + R_1}{-(L_1 + L_{1e})} & \frac{1}{-(L_1 + L_{1e})} & \frac{R_c}{(L_1 + L_{1e})} \\ \frac{1}{C + C_e} - \beta & 0 & \frac{1}{-(C + C_e)} \\ \frac{R_c}{L_2 + L_{2e}} & \frac{1}{L_2 + L_{2e}} - \psi & \frac{R_c + R_2}{-(L_2 + L_{2e})} \end{pmatrix},$$

$$T_{cm} = \begin{bmatrix} \frac{1}{L_1 + L_{1e}} - \alpha \\ 0 \\ 0 \end{bmatrix}, \quad \lambda = \begin{pmatrix} \alpha & 0 & 0 \\ 0 & \beta & 0 \\ 0 & 0 & \psi \end{pmatrix}, \quad T_{gcm} = \begin{bmatrix} 0 \\ 0 \\ \frac{1}{L_2 + L_{2e}} \end{bmatrix},$$

where $m_v = [v_{inv}, i_1, v_c]^T$. α, β, Ψ are designed as non-physical scale factors. Normally, α, β, Ψ are $1/L_1, 1/C, 1/L_2$, respectively.

To simplify the input and output of the load dynamic equation of the GCC with a LCL filter based on the ultra-local model, $\Gamma_m = [F, D, H]^T$ is defined. It subsumes little known parts of the plant as well as of the various possible system disturbances. Then, Eq. (9) can be rewritten as

$$\frac{dx}{dt} = \Gamma_m + \lambda m_v. \quad (10)$$

For the whole system, v_{inv} and i_g represent the input and output variables of the controller, respectively, while F, D and H refer to the known and unknown parts of the system. The proposed MFPC state equation of the system can be discretized accurately. Then, the discrete equation of the system is obtained as follows:

$$x(k+1) = \hat{\Gamma}_m + \lambda m_v(k) + x(k). \quad (11)$$

Equation (11) will contain the discretized predictive control equation used in Fig. 3. The detailed prediction process steps are as follows: firstly, the inductance current $i_1(k+1)$ shall be calculated according to the inverter output voltage vector $v_{inv}(k)$ and the sampled current $i_1(k)$ at the inverter side; then, according to the predicted inductance current $i_1(k+1)$ and the sampled output capacitor voltage $v_c(k)$ and the virtual capacitor voltage $v_{vr}(k)$ at the current time, the predicted capacitor voltage $v_c(k+1)$ is calculated; finally, according to the predicted capacitor voltage $v_c(k+1)$ and the sampled grid current $i_g(k)$, the predicted grid current $i_g(k+1)$ is

calculated. The concrete prediction equation is given as (12).

$$\begin{cases} \mathbf{i}_1(k+1) = T \left(\widehat{F}(k) + \alpha \mathbf{v}_{\text{inv}}(k) \right) + \mathbf{i}_1(k) \\ \mathbf{v}_c(k+1) = T \left(\widehat{D}(k) + \beta \mathbf{i}_1(k+1) \right) + \mathbf{v}_c(k) + \mathbf{v}_{vr}(k), \\ \mathbf{i}_g(k+1) = T \left(\widehat{H}(k) + \psi \mathbf{v}_c(k+1) \right) + \mathbf{i}_g(k) \end{cases} \quad (12)$$

where $\mathbf{v}_{vr}(k) = (\mathbf{i}_1(k+1) - \mathbf{i}_g(k))R_v$.

There is a sampling step delay in the actual predictive control process. To obtain grid current at $(k+2)$ -th, the discretized model free predictive control equation of the grid current is predicted again using the predictive model, (12), and reorganized as:

$$\mathbf{i}_g(k+2) = \boldsymbol{\eta}_1 \widehat{\boldsymbol{\Gamma}}_m + \boldsymbol{\eta}_2 [\mathbf{v}_{\text{inv}}(k+1), \mathbf{i}_1(k+1), \mathbf{v}_c(k+1), \mathbf{i}_g(k+1)]^T, \quad (13)$$

where: $\mathbf{v}_{\text{inv}}(k+1)$, $\mathbf{i}_1(k+1)$, $\mathbf{v}_c(k+1)$, $\mathbf{i}_g(k+1)$ are the output voltage of the converter side, the output current of the converter side, the filter capacitance voltage and the grid current at the $k+1$ time, $\boldsymbol{\eta}_1 = [\beta\Psi/T^3, \Psi/T^2, 1/T]$, $\boldsymbol{\eta}_2 = [\alpha\beta\Psi/T^3, \beta\Psi/T^2, \Psi/T, 1]$, T is the control period. $\widehat{\boldsymbol{\Gamma}}_m$ in the above formula will be discussed in detail in the next section.

4.2. Online estimation of $\widehat{\boldsymbol{\Gamma}}_m$

Based on the algebraic parameter identification technique, it is assumed that the constant function $\widehat{\boldsymbol{\Gamma}}_m$ with short time intervals is used to approximate $\boldsymbol{\Gamma}_m$. Equation (9) can be rewritten in the operation domain by the Laplace transform as

$$s\mathbf{X} = \frac{1}{s}\widehat{\boldsymbol{\Gamma}}_m + \lambda\mathbf{M}_v + \mathbf{x}(0), \quad (14)$$

where $\mathbf{x}(0) = [\mathbf{i}_1(0), \mathbf{v}_c(0), \mathbf{i}_g(0)]$ are the initial conditions that can be eliminated by taking a derivative with respect to s .

$$\mathbf{X} + s \frac{d\mathbf{X}}{ds} = -\frac{1}{s^2}\widehat{\boldsymbol{\Gamma}}_m + \frac{d(\lambda\mathbf{M}_v)}{ds}. \quad (15)$$

In order to improve the system type and attenuate the noise, the two sides of Formula (15) are multiplied by s^{-2} .

$$s^{-4}\widehat{\boldsymbol{\Gamma}}_m = -s^{-2}\mathbf{X} - s^{-1} \frac{d}{ds}\mathbf{X} + s^{-2} \frac{d(\lambda\mathbf{M}_v)}{ds}. \quad (16)$$

Equation (16) in short interval $[0, T_s]$ is simplified by the inverse Laplace transform

$$\widehat{\boldsymbol{\Gamma}}_m = -\frac{3!}{T_s^3} \int_0^{T_s} [(T_s - 2\tau)\mathbf{x}(\tau) + \lambda\tau(T_s - \tau)\mathbf{m}_v(\tau)] d\tau, \quad (17)$$

where: $T_s = n_s T$, n_s is the window sequence length and T is the sampling time.

Then, the numerical solution of the first-order integrator in (17) is realized by using the compound trapezoid formula, and its digital implementation is given as

$$\begin{aligned} \widehat{\Gamma}_m = & -\frac{3}{n_s^3 T} \sum_{\xi=1}^{n_s} ((n_s - 2(\xi - 1)) \times x[\xi - 1] \\ & + \lambda(\xi - 1)T(n_s - (\xi - 1)) \times m_v[\xi - 1] + (n_s - 2\xi) \times x[\xi] + \lambda\xi T(n_s - \xi)m_v[\xi]), \end{aligned} \quad (18)$$

where $\xi = [m, n, h]$. “ m ” represents the (m)-th sampling points, “ n ” represents the (n)-th sampling points, “ h ” represents the (h)-th sampling points.

All the above are the control design of the LCL-filtered GCC based on the ultra-local model. The nonlinear and parameter mismatch of the converter are considered in the drive system. At the same time, the proposed $\Gamma_m = [F, D, H]^T$ makes the input-output relationship of the (9) simple and intuitive. More importantly, it has strong robustness when the model parameters do not match.

For the normal MFPCC interrupt service routine, firstly, the parameters of the controller are initialized. Secondly, it is necessary to measure the current instant electrical variables such as $v_{inv}(k)$, $i_1(k)$, $v_c(k)$, $i_g(k)$, (For simplicity, these variables are represented in vector form). These voltage and current variables are input into the established ultra-local model dynamic equation shown in (9). Next, the grid current is predicted by using the instantaneous voltage and current values. The estimated model $\widehat{\Gamma}_m$ is updated continuously using (18) to keep track of any changes in the physical system, and it is used to predict the grid current at the future sampling period $k + 2$ using (13). Finally, Fig. 4 shows the estimation results of $\widehat{\Gamma}_m = [\widehat{F}, \widehat{D}, \widehat{H}]$ in the static $\alpha\beta$ coordinate system, where $\widehat{F} = \widehat{F}_\alpha + j\widehat{F}_\beta$, $\widehat{D} = \widehat{D}_\alpha + j\widehat{D}_\beta$, $\widehat{H} = \widehat{H}_\alpha + j\widehat{H}_\beta$.

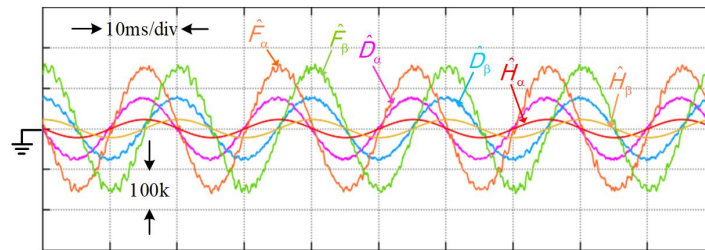


Fig. 4. Online algebraic parameter identification results

4.3. Damping method for GCC with LCL filter

According to the block diagram of the LCL filter with a series damping resistance control system in Fig. 3, the transfer function of the LCL filter with the damping resistance R_c is shown in (19).

$$G_d(s) = \frac{i_g(s)}{v_{inv}(s)} = \frac{sCR_c + 1}{s^3 L_1 CL_2 + s^2 CR_c(L_1 + L_2) + s(L_1 + L_2)}. \quad (19)$$

Since the LCL filter is a third-order system, there is a resonance peak, which is easy to cause system oscillation [27]. To solve this problem, most of the resonance damping strategies that have been proposed to date use voltage or current feedback-based setups [4–6]. Generally, these methods need to calculate the converter current reference value and capacitor voltage reference value by using the grid-current reference value. The active damping is implemented in the calculation of the reference value. Additionally, the circuit model parameters need to be used in the process of calculating the reference value. Therefore, these damping schemes are affected by the uncertainty of model parameters, which are not directly applicable to MFPCC.

The concept of virtual resistance is very common in the harmonic suppression scheme of the LCL-filtered GCC [8]. We can use an appropriate control algorithm, and introduce virtual resistance from the control loop to improve the system robustness. To maintain a balance between high-frequency stability margin and damping loss, a small passive damping resistance ($R_c = 2 \Omega$) is retained [7]. The derivation of this hybrid damping method is shown in (20)–(22).

As can be seen from the s -domain block diagram for the LCL filter, the transfer function of (18) is valid.

$$i_1(s) - i_g(s) = \frac{sCv_c(s)}{sR_cC + 1}. \quad (20)$$

From (20) it can be deduced that

$$\frac{1}{sC}i_c(s) + i_c(s)R_c = v_c(s), \quad (21)$$

where the capacitor current $i_c(s) = i_1(s) - i_g(s)$.

It is found from (21) that the effect of the term including the damping resistance R_c can be equivalent by an additional virtual capacitor voltage $v_{vr}(s)$. The equivalent result is presented in (22).

$$\frac{1}{sC}i_c(s) + v_{vr}(s) = v_c(s) \quad (22)$$

with

$$v_{vr}(s) = R_{vr}i_c(s),$$

where the damping resistance $R_{vr} = R_v + R_c$, which means that the virtual resistance R_v is added under the condition of retaining a small resistance, R_c , to enhance the damping effect and reduce the circuit loss.

Figure 5 expresses the main structure of the additive virtual resistance in the s -domain. The transfer function from the grid current $i_g(s)$ to the converter output voltage $v_{inv}(s)$ can be expressed as

$$G_{vd}(s) = \frac{i_g(s)}{v_{inv}(s)} = \frac{G_{vp}(s)}{s^2L_1L_2 + sR_c(L_1 + L_2) + (L_1 + L_2)/C}, \quad (23)$$

where the transfer function from capacitor voltage to capacitor current can be expressed as $G_{vp}(s) = (sCR_{vr} + 1)/sC$.

The damping effect after adding the virtual damping resistance is shown by the Bode diagram in Fig. 6. It can be seen from the plan that the LCL filter presents a resonance peak higher than 0 dB at the resonance frequency and the phase jumps from -90° to -270° , which very easy causes the system instability in the undamped state. Although the small passive damping resistance can

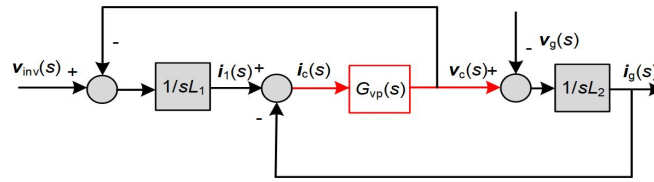


Fig. 5. Block diagram of LCL filter with a virtual damping resistance

reduce the energy loss, its damping effect is not noticeable. When the virtual resistance R_v is added to the controller, the resonance peak value can be greatly reduced. As a result, the system can operate safely and stably and the resonance problem can be well solved.

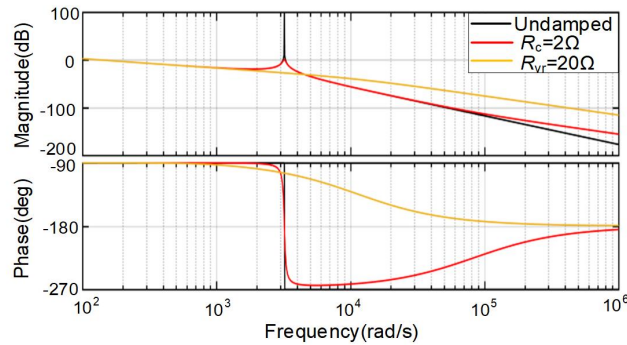


Fig. 6. Bode plots of LCL filter transfer functions with a virtual resistance

For the MFPCC of the LCL-filtered GCC, this paper designs the damping scheme of the system from the point of view of the controller to avoid the resonance of the system. This method is simple and effective, and enhance the stability of the system. The detailed implementation method of the proposed damping scheme is depicted in Fig. 3. In a word, the proposed method can not only suppress the resonance of the filter, but also solve the dependence of model predictive control on parameters, and realize the MFPCC of the LCL-filtered GCC.

5. Experimental results

To evaluate the performance of the proposed method and the power quality of the grid-side current, an experimental platform is designed as shown in Fig. 7, which includes a simulator of Typhoon602+ and a controller of PE-Expert4. The proposed control algorithm is implemented using the PE-Expert4 processor board, which consists of DSP and FPGA control chips. The parameters of the experimental platform are tabulated in Table 1.

Table 1. Simulation and experimental parameters

Symbol	Parameters	Values
U_{dc}	DC voltage	500 V
v_g	Grid phase voltage (RMS)	120 V
L_1	Converter side filter inductor	2.4 mH
C	Filter capacitor	60 μ F
L_2	Grid-side filter inductor	5 mH
R_v	Virtual resistance	18 Ω
T	Sampling time	25 μ s
f	Grid frequency	50 Hz

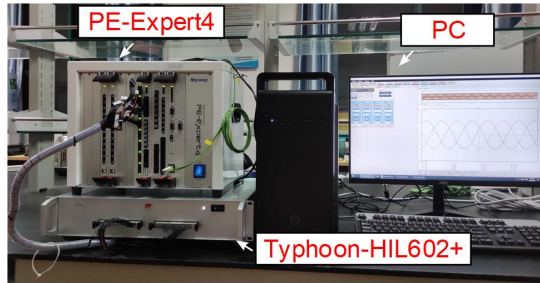


Fig. 7. Photograph of the experimental setup

5.1. Performance testing with matched model parameters

According to the theoretical analysis in section 4.3, the experimental results of grid current with and without a virtual damping resistance are shown in Fig. 8. It can be observed from Fig. 8(a) that the grid current immediately resonates when the virtual resistance suddenly fails. From Fig. 8(b), it can be found that the resonance of the grid connected current disappears and reaches a stable operating state when the virtual resistance is suddenly added. This shows that the proposed virtual damping method eliminates the high-frequency component of grid current and suppresses the system resonance.

When the model parameters are matched, the conventional predictive grid-current control and the proposed model-free predictive grid current are dynamically tested. Then the harmonic spectrum of grid current is compared and analyzed.

Figure 9 shows the dynamic experimental waveform of three-phase grid current and β phase current when the reference current changes suddenly from 6 A to 10 A. It can be seen from Fig. 9(a)–(b) that both methods can quickly track the reference current, meaning that both of the two methods have good dynamic characteristics.

The fast Fourier transform (FFT) analysis results corresponding to Fig. 9 are shown in Fig. 10. When the grid current is 6 A and 10 A, respectively, the current THD of conventional MPC is

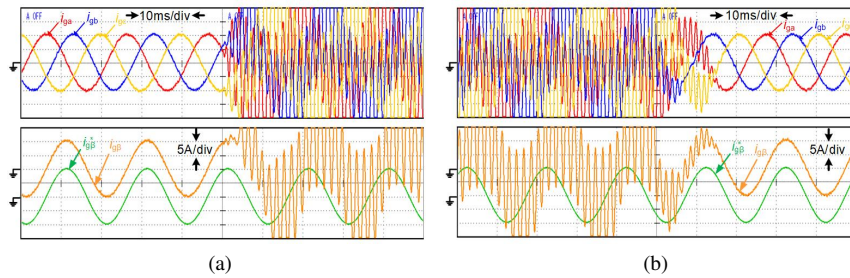


Fig. 8. The experimental results of grid connected current with and without a virtual damping resistance: (a) virtual damping resistance from presence to absence; (b) virtual damping resistance from absence to presence

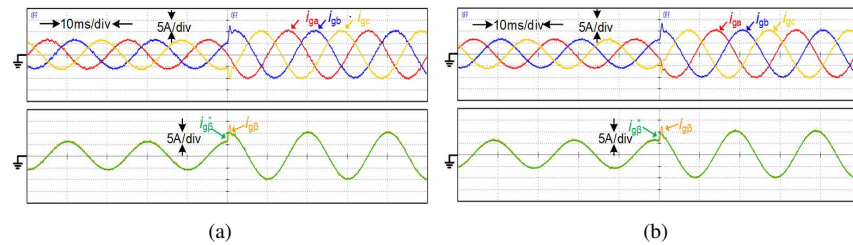


Fig. 9. Experimental comparisons of dynamic performance (6 A/10 A): (a) conventional grid-connected current MPC; (b) proposed MFPC

4.63% and 2.99%, respectively, as shown in Fig. 10(a). However, Fig. 10(b) shows that the THD of the grid current decreases to 3.24% and 2.65% by using the proposed MFPC method, respectively. That means the proposed MFPC method has smaller THD under different grid-current amplitudes.

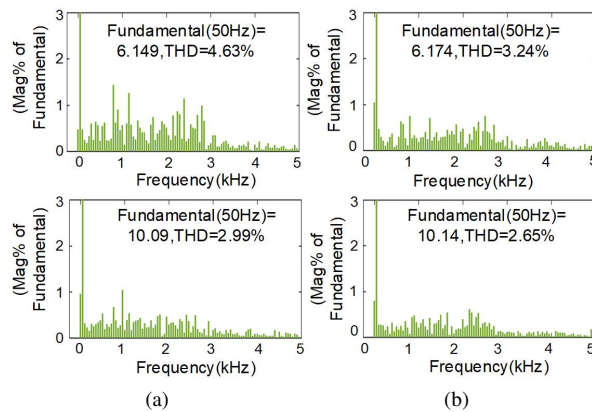


Fig. 10. Experimental comparisons of FFT analysis: (a) conventional MPC (6 A/10 A); (b) proposed MFPC (6 A/10 A)

5.2. Performance testing with mismatched model parameters

To verify the parameter robustness of the proposed control method, the control performance of the MFPCC method and conventional MPC method is compared and analyzed when the model parameters are mismatched. Figures 11(a)–(f) show the comparison results of the phase β grid-current error and FFT analysis when inductance parameters and capacitance parameters are mismatched. The system starts with the conventional MPC method, and then switches to the MFPCC method.

What is clearly presented in Fig. 11 is that the THD of the conventional MPC method is larger than the proposed control method when the model parameters are mismatched. This is because the increase of current error will affect the selection of the optimal voltage vector in MPC. If the switching state corresponding to the optimal voltage vector is not selected, the current waveform will deteriorate. In some cases of parameter mismatch, the current error of conventional MPC becomes larger.

Figures 11(a), (c), (e) show the β phase current error and FFT analysis results when the model parameters are small. It can be seen from the chart that the small model parameters have a great impact on the current error for conventional MPC, especially the grid-side inductance L_2 becomes smaller. Figures 11(b), (d), (f) show the β phase current error and FFT analysis results when the model parameters are large. It can be seen from the chart that the large model parameters have a great impact on the current THD for conventional MPC, while the MFPCC method is not affected by parameter changes.

For the sake of clarity, Table 2 is given to show the current THD and error under different parameter conditions.

Table 2. Test result of the current quality in parameters variation condition

Model parameter	Total harmonic distortion (THD)		Current error (RMS)	
	Conventional MPC	MFPCC	Conventional MPC	MFPCC
$L_1 = 1.2$ mH, $C = 30$ μ F	2.94%	2.65%	0.42 A	0.39 A
$L_1 = 4.8$ mH, $C = 90$ μ F	3.42%	2.65%	0.45 A	0.39 A
$L_1 = 1.2$ mH, $L_2 = 2.5$ mH	3.01%	2.65%	0.49 A	0.39 A
$L_1 = 4.8$ mH, $L_2 = 6.5$ mH	4.02%	2.65%	0.44 A	0.39 A
$C = 30$ μ F, $L_2 = 2.5$ mH	3.46%	2.65%	0.63 A	0.39 A
$C = 90$ μ F, $L_2 = 6.5$ mH	4.32%	2.65%	0.46 A	0.39 A

It can be found that the conventional MPC control method is greatly affected by the change of model parameters. The maximum error root mean square (RMS) of steady-state current is 0.63 A

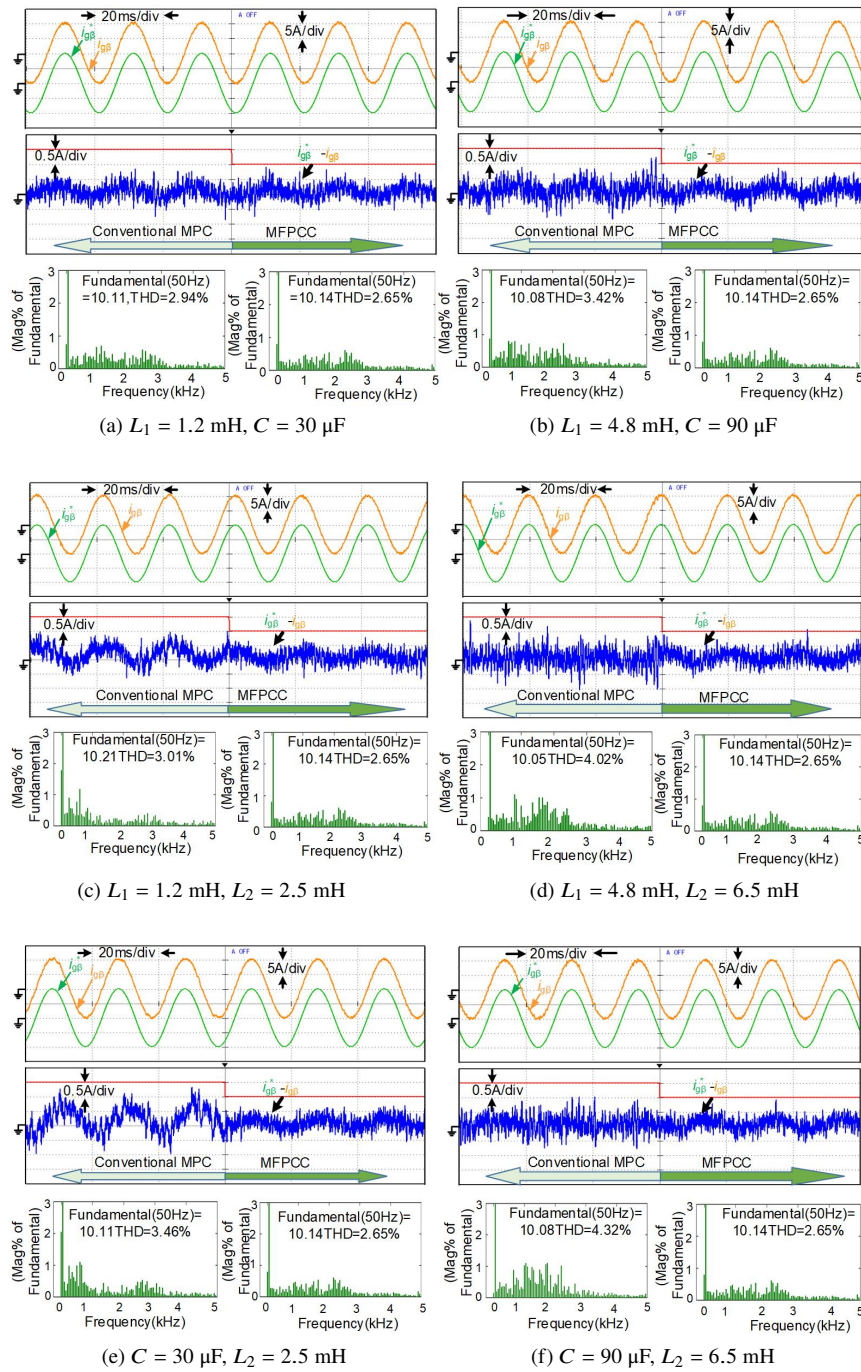


Fig. 11. Experimental comparison of grid-current control performance between two control methods when model parameters are mismatched

and the maximum THD of grid current achieves 4.32% for conventional MPC, while the MFPC method proposed in this paper is not affected by the change of model parameters. Experiments results indicate that the proposed method has strong parameter robustness.

6. Conclusion

This paper proposed a MFPC algorithm based on an ultra-local model for an LCL-filtered GCC, which presents strong parameter robustness. First, the LCL filter circuit model and the conventional grid-current MPC method are introduced. When the filter parameters are mismatched, the influence of the filter parameters on the current prediction error is analyzed. In view of this, based on the established ultra-local model, a model-free grid-current prediction controller is designed. Meanwhile, an active damping scheme is studied to suppress the system inherent resonance. The proposed MFPC scheme has smaller current THD than the conventional MPC with matched model parameters. Moreover, when the LCL filter parameters do not match, the proposed control method can still reduce the grid-side current error and THD obviously compared with the conventional MPC control method. Experimental results have verified the effectiveness of the proposed method.

Acknowledgements

This work was supported in part by the National Natural Science Foundation of China (51907046), in part by the Scientific and Technological Project in Henan Province (212102210021) in part by the Youth Talent Support Project of Henan Province (2019HYTP021).

References

- [1] Agüero J.R., Takayesu E., Novosel D., Masiello R., *Modernizing the grid: challenges and opportunities for a sustainable future*, IEEE Power and Energy Magazine, vol. 15, no. 3, pp. 74–83 (2017), DOI: [10.1109/MPE.2017.2660819](https://doi.org/10.1109/MPE.2017.2660819).
- [2] Wu W., Huang M., Blaabjerg F., *Efficiency comparison between the LLCL and LCL-filters based single-phase grid-tied inverters*, Archives of Electrical Engineering, vol. 63, no. 1, pp. 63–79 (2014), DOI: [10.2478/ae-2014-0005](https://doi.org/10.2478/ae-2014-0005).
- [3] Reznik A., Simões M.G., Al-Durra A., Muyeen S.M., *LCL filter design and performance analysis for grid-interconnected systems*, IEEE Transactions on Industry Applications, vol. 50, no. 2, pp. 1225–1232 (2014), DOI: [10.1109/TIA.2013.2274612](https://doi.org/10.1109/TIA.2013.2274612).
- [4] Falkowski P., Sikorski A., *Finite control set model predictive control for grid-connected AC–DC converters with LCL filter*, IEEE Transactions on Industrial Electronics, vol. 65, no. 4, pp. 2844–2852 (2018), DOI: [10.1109/TIE.2017.2750627](https://doi.org/10.1109/TIE.2017.2750627).
- [5] Panten N., Hoffmann N., Fuchs F.W., *Finite control set model predictive current control for grid-connected voltage-source converters with LCL filters: a study based on different state feedbacks*, IEEE Transactions on Power Electronics, vol. 31, no. 7, pp. 5189–5200 (2016), DOI: [10.1109/TPEL.2015.2478862](https://doi.org/10.1109/TPEL.2015.2478862).
- [6] Xu J., Xie S., Tang T., *Active damping-based control for grid-connected LCL-filtered inverter with injected grid-current feedback only*, IEEE Transactions on Industrial Electronics, vol. 61, no. 9, pp. 4746–4758 (2014), DOI: [10.1109/TIE.2013.2290771](https://doi.org/10.1109/TIE.2013.2290771).

- [7] Liu H., Xu D., Li L., Gao Q., *A robust damping method for voltage source converter with LCL filter under weak grid*, CSEE Journal of Power and Energy Systems, pp. 1–9 (2020), DOI: [10.17775/CS EEJPES.2019.02400](https://doi.org/10.17775/CS EEJPES.2019.02400).
- [8] Scoltock J., Geyer T., Madawala U.K., *A model predictive direct current control strategy with predictive references for MV grid-connected converters with LCL-filters*, IEEE Transactions on Power Electronics, vol. 30, no. 10, pp. 5926–5937 (2015), DOI: [10.1109/TPEL.2014.2375919](https://doi.org/10.1109/TPEL.2014.2375919).
- [9] Wang X., Wang Z., Xu Z., Wang W., Wang B., Zou Z., *Deadbeat Predictive Current Control-Based Fault-Tolerant Scheme for Dual Three-Phase PMSM Drives*, IEEE Journal of Emerging and Selected Topics in Power Electronics, vol. 9, no. 2, pp. 1591–1604 (2021), DOI: [10.1109/JESTPE.2020.2983691](https://doi.org/10.1109/JESTPE.2020.2983691).
- [10] Kalla U.K., Kaushik H., Singh B., Kumar S., *Adaptive control of voltage source converter based scheme for power quality improved grid-interactive solar PV-battery system*, IEEE Transactions on Industry Applications, vol. 56, no. 1, pp. 787–799 (2020), DOI: [10.1109/TIA.2019.2947397](https://doi.org/10.1109/TIA.2019.2947397).
- [11] Hu J., Shang L., He Y., Zhu Z.Q., *Direct active and reactive power regulation of grid-connected DC/AC converters using sliding mode control approach*, IEEE Transactions on Power Electronics, vol. 26, no. 1, pp. 210–222 (2011), DOI: [10.1109/TPEL.2010.2057518](https://doi.org/10.1109/TPEL.2010.2057518).
- [12] Tang M., Yang S., Zhang K. *et al.*, *Model predictive direct power control of energy storage quasi-Z-source grid-connected inverter*, Archives of Electrical Engineering, vol. 71, no. 1, pp. 21–35 (2022), DOI: [10.24425/ae.2022.140195](https://doi.org/10.24425/ae.2022.140195).
- [13] Karamanakos P., Liegmann E., Geyer T., Kennel R., *Model predictive control of power electronic systems: methods, results, and challenges*, IEEE Open Journal of Industry Applications, vol. 1, pp. 95–114 (2020), DOI: [10.1109/OJIA.2020.3020184](https://doi.org/10.1109/OJIA.2020.3020184).
- [14] Guo L., Jin N., Li Y., Luo K., *A model predictive control method for grid-connected power converters without AC voltage sensors*, IEEE Transactions on Industrial Electronics, vol. 68, no. 2, pp. 1299–1310 (2021), DOI: [10.1109/TIE.2020.2970638](https://doi.org/10.1109/TIE.2020.2970638).
- [15] Geldenhuys J.M.C., du Toit Mouton H., Rix A., Geyer T., *Model predictive current control of a grid connected converter with LCL-filter*, 2016 IEEE 17th Workshop on Control and Modeling for Power Electronics (COMPEL), Trondheim, Norway, pp. 1–6 (2016), DOI: [10.1109/COMPEL.2016.7556734](https://doi.org/10.1109/COMPEL.2016.7556734).
- [16] Young H.A., Perez M.A., Rodriguez J., *Analysis of finite-control-set model predictive current control with model parameter mismatch in a three-phase inverter*, IEEE Transactions on Industrial Electronics, vol. 63, no. 5, pp. 3100–3107 (2016), DOI: [10.1109/TIE.2016.2515072](https://doi.org/10.1109/TIE.2016.2515072).
- [17] Guo L., Xu Z., Jin N., Chen Y., Li Y., Dou Z., *An inductance on-line identification method for model predictive control of V2G inverter with enhanced robustness to grid frequency deviation*, IEEE Transactions on Transportation Electrification, DOI: [10.1109/TTE.2021.3128362](https://doi.org/10.1109/TTE.2021.3128362).
- [18] Guo L., Xu Z., Li Y., Chen Y., Jin N., Lu F., *An inductance online identification-based model predictive control method for grid-connected inverters with an improved phase-locked loop*, IEEE Transactions on Transportation Electrification, vol. 8, iss. 2, pp. 2695–2709 (2022), DOI: [10.1109/TTE.2021.3135326](https://doi.org/10.1109/TTE.2021.3135326).
- [19] Shen K., Zhang J., *Modeling error compensation in FCS-MPC of a three-phase inverter*, 2012 IEEE International Conference on Power Electronics, Drives and Energy Systems (PEDES), Bengaluru, India, pp. 1–6 (2012), DOI: [10.1109/PEDES.2012.6484341](https://doi.org/10.1109/PEDES.2012.6484341).
- [20] Mendez R., Sbarbaro D., Espinoza J., *High dynamic and static performance FCS-MPC strategy for static power converters*, 2016 IEEE Energy Conversion Congress and Exposition (ECCE), Milwaukee WI, USA, pp. 1–7 (2016), DOI: [10.1109/ECCE.2016.7855146](https://doi.org/10.1109/ECCE.2016.7855146).
- [21] Yang Y., Tan S., Hui S.Y.R., *Adaptive reference model predictive control with improved performance for voltage-source inverters*, IEEE Transactions on Control Systems Technology, vol. 26, no. 2, pp. 724–731 (2018), DOI: [10.1109/TCST.2017.2670529](https://doi.org/10.1109/TCST.2017.2670529).

- [22] Jabbour N., Mademlis C., *Online parameters estimation and autotuning of a discrete-time model predictive speed controller for induction motor drives*, IEEE Transactions on Power Electronics, vol. 34, no. 2, pp. 1548–1559 (2019), DOI: [10.1109/TPEL.2018.2831459](https://doi.org/10.1109/TPEL.2018.2831459).
- [23] Lin C.K., Liu T.H., Yu J.T., Fu L.C., Hsiao C.F., *Model-free predictive current control for interior permanent-magnet synchronous motor drives based on current difference detection technique*, IEEE Transactions on Industrial Electronics, vol. 61, no. 2, pp. 667–681 (2014), DOI: [10.1109/TIE.2013.2253065](https://doi.org/10.1109/TIE.2013.2253065).
- [24] Zhou Y., Li H., Zhang H., *Model-free deadbeat predictive current control of a surface-mounted permanent magnet synchronous motor drive system*, Journal of Power Electronics, vol. 18, no. 1, pp. 103–115 (2018), DOI: [10.6113/JPE.2018.18.1.103](https://doi.org/10.6113/JPE.2018.18.1.103).
- [25] Yuan X., Zuo Y., Fan Y., Lee C.H.T., *Model-free predictive current control of SPMSM drives using extended state observer*, IEEE Transactions on Industrial Electronics, vol. 69, no. 7, pp. 6540–6550 (2022), DOI: [10.1109/TIE.2021.3095816](https://doi.org/10.1109/TIE.2021.3095816).
- [26] Zhang Y., Jiang T., Jiao J., *Model-free predictive current control of a DFIG using an ultra-local model for grid synchronization and power regulation*, IEEE Transactions on Energy Conversion, vol. 35, no. 4, pp. 2269–2280 (2020), DOI: [10.1109/TEC.2020.3004567](https://doi.org/10.1109/TEC.2020.3004567).
- [27] Xu J., Xie S., *LCL-resonance damping strategies for grid-connected inverters with LCL filters: a comprehensive review*, Journal of Modern Power Systems and Clean Energy, vol. 6, no. 2, pp. 292–305 (2018), DOI: [10.1007/s40565-017-0319-7](https://doi.org/10.1007/s40565-017-0319-7).